DOI: 10.1002/chem.200701124

Directed Synthesis of a Heterobimetallic Complex Based on a Novel Unsymmetric Double-Schiff-Base Ligand: Preparation, Characterization, Reactivity and Structures of Hetero- and Homobimetallic Nickel(II) and Zinc(II) Complexes

Arne Roth,[a] Axel Buchholz,[a] Manfred Rudolph,[a] Eileen Schütze,[b] Erika Kothe,[b] and Winfried Plass*[a]

Abstract: A series of bimetallic zinc(II) and nickel(II) complexes based on the novel dinucleating unsymmetric double-Schiff-base ligand benzoic acid [1-(3-{[2-(bispyridin-2-ylmethylamino)-ethylimino]methyl}-2-hydroxy-5-methylphenyl)methylidene]hydrazide (H_2bpampbh) has been synthesized and structurally characterized. The metal centers reside in two entirely different binding pockets provided by the ligand H_2bpampbh, a planar tridentate [ONO] and a pentadentate [ON_4] compartment. The utilized ligand H_2bpampbh has been synthesized by condensation of the single-Schiff-base proligand Hbpahmb with benzoic acid hydrazide. The reaction of H_2bpampbh with two equivalents of either zinc(II) or nickel(II) acetate yields the homobimetallic complexes [Zn_2(bpampbh)-(μ,η^1-OAc)(η^1-OAc)] (**ZnZn**) and [Ni_2-(bpampbh)(μ-H_2O)(η^1-OAc)(H_2O)]-(OAc) (**NiNi**), respectively. Simultaneous presence of one equivalent zinc(II) and one equivalent nickel(II) acetate results in the directed formation of the heterobimetallic complex [NiZn-(bpampbh)(μ,η^1-OAc)(η^1-OAc)] (**NiZn**) with a selective binding of the nickel ions in the pentadentate ligand compartment. In addition, two homobimetallic azide-bridged complexes [Ni_2-(bpampbh)(μ,η^1-N_3)]ClO_4 (**NiNi(N_3)**) and [Ni_2(bpampbh)(μ,η^1-N_3)($MeOH)_2$]-$(ClO_4)_{0.5}(N_3)_{0.5}$ (**NiNi(N_3)(MeOH)$_2$**) were synthesized. In all complexes, the metal ions residing in the pentadentate compartment adopt a distorted octahedral coordination geometry, whereas the metal centers placed in the tridentate compartment vary in coordination number and geometry from square-planar (**NiNi(N_3)**) and square-pyramidal (**ZnZn** and **NiZn**), to octahedral (**NiNi** and **NiNi(N_3)(MeOH)$_2$**). In the case of complex **NiNi(N_3)** this leads to a mixed-spin homodinuclear nickel(II) complex. All compounds have been characterized by means of mass spectrometry as well as IR and UV/Vis spectroscopies. Magnetic susceptibility measurements show significant zero-field splitting for the nickel-containing complexes ($D = 2.9$ for **NiZn**, 2.2 for **NiNi(N_3)**, and 0.8 cm^{-1} for **NiNi**) and additionally a weak antiferromagnetic coupling ($J = -1.4$ cm^{-1}) in case of **NiNi**. Electrochemical measurements and photometric titrations reveal a strong Lewis acidity of the metal center placed in the tridentate binding compartment towards external donor molecules. A significant superoxide dismutase reactivity against superoxide radicals was found for complex **NiNi**.

Keywords: bioinorganic chemistry · directed synthesis · heterometallic complexes · magnetic properties · unsymmetric dinucleating ligands

Introduction

Metalloenzymes containing dinuclear reactive centers are widely spread in biological systems and numerous examples of such enzymes with homo- or heterometallic centers have been structurally characterized (for selected reviews, see[1–3]). As an important feature of homo- and heterodinuclear active sites of metalloenzymes, the surrounding protein matrix usually provides chemically distinct binding environments for the individual metal centers, commonly referred

[a] A. Roth, Dr. A. Buchholz, Dr. M. Rudolph, Prof. Dr. W. Plass
Institut für Anorganische und Analytische Chemie
Friedrich-Schiller-Universität Jena
Carl-Zeiss-Promenade 10, 07745 Jena (Germany)
Fax: (+49) 3641-948132
E-mail: sekr.plass@uni-jena.de

[b] E. Schütze, Prof. Dr. E. Kothe
Institut für Mikrobiologie, Friedrich-Schiller-Universität Jena
Neugasse 25, 07743 Jena (Germany)

Supporting information for this article is available on the WWW under http://www.chemeurj.org/ or from the author.

to as site asymmetry at metallobiosites.[4] Differences in ligand types, as well as in coordination numbers and geometries, can contribute to this asymmetry,[5] thus enabling two metal centers (even in homodinuclear cases) to perform different tasks in the enzymatic reactions. Common examples of metalloenzymes with homobimetallic unsymmetric active sites are urease[6] (Ni_2) and the dioxygen carrier hemerythrin[7] (Fe_2), whereas the iron–zinc purple acid phosphatases[8] and copper–zinc superoxide dismutase[9] represent enzymatic systems containing unsymmetric heterobimetallic metallobiosites. It is clear for these systems, that the lack of symmetry of the active center is a very important structural feature of such enzymes and decisive for the catalytic mechanism. Accordingly, the asymmetry of the binding environment should be taken into account for the design of bioinorganic model compounds. Indeed, the search for designed unsymmetric dinucleating model systems has been an extensive area of research over the last decades.

An effective way to obtain such complexes is the application of dinucleating ligands providing two chemically different binding compartments (for selected examples and reviews, see references [10–20]). Unfortunately, the accessibility of such unsymmetric ligands is often hampered by various synthetic problems, which is the simple reason for the fact that the majority of the presently known bioinorganic model complexes are symmetric.

A simple, straight-forward, and versatile synthetic access towards unsymmetric "end-off" double-Schiff-base ligands has recently been reported by us.[21] The method is based on the stepwise Schiff-base formation that utilizes a symmetric dicarbonyl bridge and two primary amines. After the first reaction step, the monocarbonyl proligand is separated from the symmetric side products by size-exclusion chromatography, and reaction of the isolated proligand with a second amine yields the desired unsymmetric ligand. To demonstrate the feasibility of this method, we synthesized the proligand Hbpahmb (see Scheme 1) in high yields and purity.

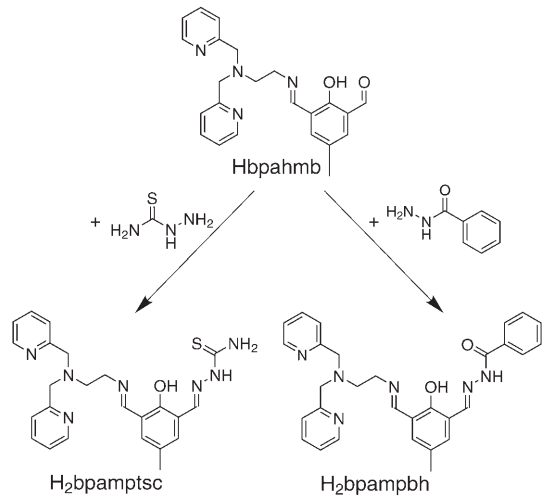

Scheme 1. Synthesis of unsymmetric double-Schiff-base ligands starting from the proligand Hbpahmb.

The first unsymmetric double-Schiff-base ligand, H_2bpamptsc (see Scheme 1), synthesized according to our synthetic route, has been obtained by treating Hbpahmb with thiosemicarbazide. We were able to show that this ligand system allows for the directed synthesis of a heterodinuclear copper–zinc complex.[21]

The present work is an extension of our effort towards the synthesis of new unsymmetric dinucleating ligand systems and their coordination compounds. Herein the synthesis of a series of homo- and heterodinuclear nickel(II) and zinc(II) complexes based on the novel unsymmetric ligand H_2bpampbh (see Scheme 1) is reported. In addition, the characterization of the structural, spectroscopic, and chemical properties of these compounds is subject of the present work.

Results and Discussion

Synthesis: The ligand H_2bpampbh is obtained by stoichiometric reaction of the proligand Hbpahmb with a solution of benzoic acid hydrazide in methanol (Scheme 1). The H_2bpampbh ligand provides two entirely different binding pockets, a planar tridentate [ONO] hydrazide compartment, formed by the benzhydrazide arm, and a pentadentate [ON_4] amine compartment, which is composed of the pyridine-functionalized ethylenediamine arm. Throughout this paper we will refer to the metal ions bound to these compartments as hydrazide-bound and amine-bound metal center, respectively.

For the synthesis of the homodinuclear metal complexes [Zn_2(bpampbh)(μ,η^1-OAc)(η^1-OAc)] (**ZnZn**) and [Ni_2-(bpampbh)(μ-H_2O)(η^1-OAc)(H_2O)](OAc) (**NiNi**), solutions of the H_2bpampbh ligand in acetonitrile are reacted with two equivalents metal(II) acetate dispersed in acetonitrile in the presence of two equivalents of triethylamine (Scheme 2). In case of the heterodinuclear complex [NiZn-(bpampbh)(μ,η^1-OAc)(η^1-OAc)] (**NiZn**), H_2bpampbh is reacted simultaneously with equimolar amounts of nickel(II) and zinc(II) acetate dispersed in acetonitrile. In all reactions, the metal salts dissolved completely upon complexation, accompanied by a color change from dark yellow to red-brown in case of the nickel-containing systems and bright yellow in case of the homobimetallic zinc compound. The complexes can be crystallized at −20 °C directly from the reaction solutions.

Two additional homobimetallic nickel complexes of H_2bpampbh are obtained by treating solutions of H_2bpampbh in acetonitrile with two equivalents of nickel(II) perchlorate in the presence of two equivalents of triethylamine, followed by addition of one equivalent of solid NaN_3. This method avoids an excess of coordinating anions by using the perchlorate salt instead of nickel(II) acetate as metal precursor. [Ni_2(bpampbh)(μ,η^1-N_3)]ClO_4 (**NiNi(N_3)**) can be isolated as crystalline material directly from the reaction solution by cooling to −20 °C or by slow evaporation of the solvent. Redissolving **NiNi(N_3)** in methanol and subse-

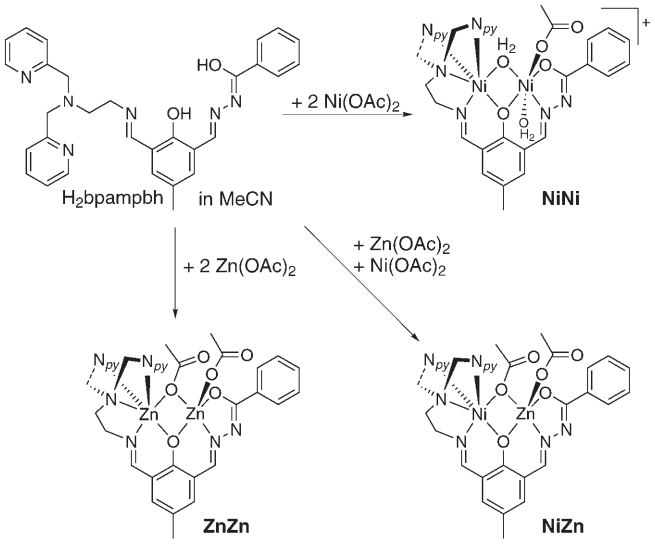

Scheme 2. Synthesis of homo- and heterobimetallic complexes utilizing the unsymmetric double-Schiff-base ligands H_2bpampbh.

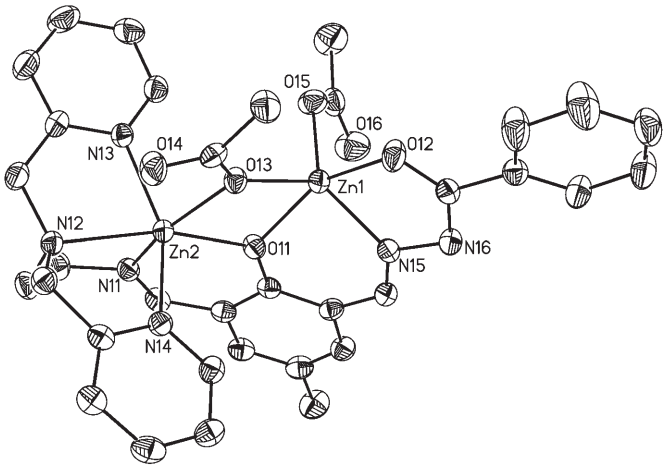

Figure 1. Molecular structure of **ZnZn** (one of three crystallographically independent molecules shown). Thermal ellipsoids are drawn at the 50% probability level. Hydrogen atoms and non-coordinated solvent molecules are omitted for clarity.

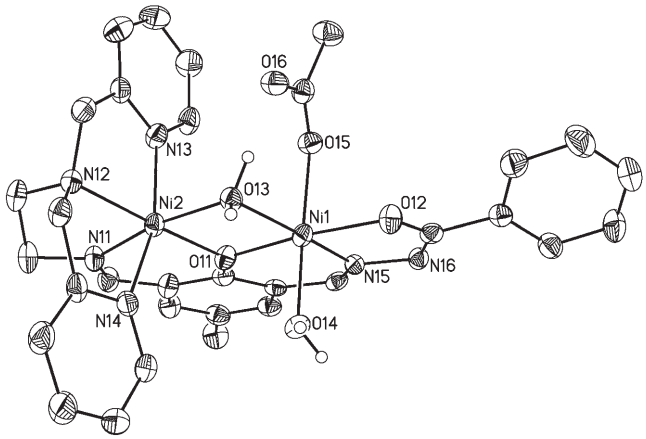

Figure 2. Molecular structure of the complex cation $[Ni_2(bpampbh)(\mu\text{-}H_2O)(\eta^1\text{-}OAc)(H_2O)]^+$ of **NiNi** (one of two crystallographically independent molecules shown). Thermal ellipsoids are drawn at the 50% probability level. Carbon-bound hydrogen atoms, anions and non-coordinated solvent molecules are omitted for clarity.

quent slow evaporation yielded the crystalline methanol adduct $[Ni_2(bpampbh)(\mu,\eta^1\text{-}N_3)(MeOH)_2](ClO_4)_{0.5}(N_3)_{0.5}$ (**NiNi(N_3)($MeOH)_2$**). It should be noted here that for all physical and chemical experiments described in this paper exclusively the azide-bridged nickel(II) complex **NiNi(N_3)** was used.

Crystal structures: The homobimetallic compounds **ZnZn** and **NiNi** crystallize in the centrosymmetric space group $P\bar{1}$ with three and two crystallographically independent chiral complex molecules per asymmetric unit, respectively. The crystallographically independent species within the crystal structures of **ZnZn** as well as **NiNi** show the same structural features, and vary only slightly in their metric parameters. Therefore, the structural details of only one independent molecule of each compound are discussed here. The molecular structures are presented in Figure 1 and Figure 2, selected bond lengths are given in Table 1.

All donor atoms of the H_2bpampbh ligand are involved in the complexation of the metal centers and the high intrinsic asymmetry of the ligand is reflected in the totally different coordination environments of the two metal centers in each compound. In all complexes discussed in this paper,

Table 1. Selected bond lengths [pm] for **ZnZn**, **NiZn**, **NiNi**, and **NiNi(N_3)($MeOH)_2$**.

ZnZn[a]		**NiZn**		**NiNi**[a]		**NiNi(N_3)($MeOH)_2$**	
Zn1–O11	210.7(2)	Zn–O1	210.8(3)	Ni1–O11	202.6(2)	Ni1–O1	202.7(3)
Zn1–O12	207.1(2)	Zn–O2	206.2(3)	Ni1–O12	201.0(2)	Ni1–O2	201.9(3)
Zn1–N15	202.7(3)	Zn–N5	205.6(4)	Ni1–N15	197.4(3)	Ni1–N5	197.6(4)
Zn1–O13	204.8(2)	Zn–O3	203.8(3)	Ni1–O13	210.1(3)	Ni1–N7	206.3(4)
Zn1–O15	193.4(3)	Zn–O5	202.5(4)	Ni1–O14	207.5(3)	Ni1–O1 M	211.7(3)
				Ni1–O15	210.1(3)	Ni1–O2 M	211.9(4)
Zn2–O11	210.7(2)	Ni–O1	204.2(3)	Ni2–O11	200.4(3)	Ni2–O1	201.8(3)
Zn2–O13	211.6(2)	Ni–O3	213.5(3)	Ni2–O13	209.9(3)	Ni2–N7	211.8(4)
Zn2–N11	210.5(3)	Ni–N1	204.4(3)	Ni2–N11	198.5(3)	Ni2–N1	199.2(4)
Zn2–N12	226.4(3)	Ni–N2	214.5(4)	Ni2–N12	208.3(3)	Ni2–N2	208.4(4)
Zn2–N13	216.3(3)	Ni–N3	207.6(3)	Ni2–N13	209.3(3)	Ni2–N3	209.0(4)
Zn2–N14	215.3(3)	Ni–N4	206.6(3)	Ni2–N14	212.2(3)	Ni2–N4	210.5(5)

[a] The metric parameters of additional crystallographically independent molecules are given in Tables S1 and S2 in the Supporting Information.

H_2bpampbh acts as dianionic ligand species with the phenolic OH and the amidic NH function being deprotonated upon complexation.

In the homobimetallic compounds **ZnZn** and **NiNi** the metal centers are bridged by the ligand phenolate oxygen atom (O11) and an additional external oxygen donor function (O13), that is, a μ,η^1-bridging acetate ion in case of **ZnZn** and a water molecule for **NiNi**. The metal–metal distances are found to be 329 (**ZnZn**) and 310 pm (**NiNi**), with bridge angles of 103 (**ZnZn**) and 101° (**NiNi**) for the phenolate bridge as well as 105 (**ZnZn**) and 95° (**NiNi**) for the external M–O13–M bridge. In the amine compartment, the four nitrogen donor functions complete the $[O_2N_4]$ coordination environment around the metal center (Zn2 or Ni2). The coordination geometry of the amine compartment may be described as strongly distorted octahedral. The extent of distortion is smaller in **NiNi** with *trans* angles ranging from 160 to 173°, as compared to a *trans* angle range of 148 to 162° in **ZnZn**. The largest deviation from a 180° *trans* angle in the amine compartment of both homobimetallic complexes is found between the metal–$N_{pyridyl}$ bonds (N13–Zn2/Ni2–N14), which can be explained by steric constraints of the pyridyl side chains. In addition, the bond lengths (see Table 1) in the amine compartment of **ZnZn**, ranging from 211 (Zn2–N11) to 226 pm (Zn2–N12), are significantly elongated compared to the corresponding parameters in **NiNi** which range from 199 (Ni2–N11) to 212 pm (Ni2–N14).

In contrast to the similarities observed for the amine compartments of both complexes, the hydrazide compartments show significant structural differences. The hydrazide-bound neutral zinc atom Zn1 in **ZnZn** is five-coordinate with an $[O_4N]$ donor set, assembled by the H_2bpampbh donor atoms, the acetate bridge and a second η^1-coordinating, non-bridging acetate ion. The non-bridging acetate ligand shows a twofold rotational disorder (see Figure S1 in the Supporting Information) in two of the three crystallographically independent complex molecules, whereas it is perfectly ordered in the third complex molecule of the crystal structure (Figure 1). The coordination geometry appears to be intermediate between square-pyramidal and trigonal-bipyramidal, as is evident from the structural index parameter τ with a value of 0.35 ($\tau = 0$ for an ideal tetragonal and 1 for a trigonal geometry).

Unlike the zinc complex, the hydrazide-bound metal atom Ni1 in **NiNi** is six-coordinate. Instead of an acetate ion, a water molecule functions as external bridge between the metal centers. A η^1-coordinating acetate ion and a second water molecule as apical ligands complete the $[O_5N]$ donor set of Ni1. The coordination geometry can be well described as slightly distorted octahedral with *trans* angles ranging from 171° (O11–Ni1–O12) to 173° (O14–Ni1–O15). As a consequence of the absence of a second coordinated acetate ligand in **NiNi**, the complex molecules are monocationic and the charge is compensated by a non-coordinated acetate ion in solid state.

The heterobimetallic complex **NiZn** crystallizes in the orthorhombic space group $P2_12_12_1$ with one chiral complex molecule per asymmetric unit. The molecular structure of **NiZn** depicted in Figure 3 (see Table 1) is highly related to the structure of the homodinuclear complex **ZnZn**, with a

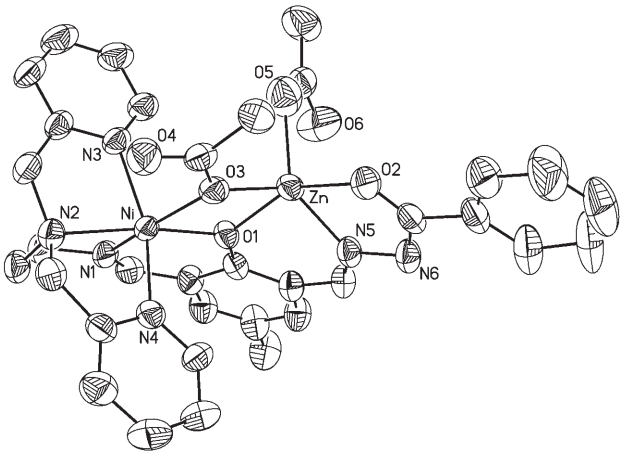

Figure 3. Molecular structure of **NiZn**. Thermal ellipsoids are drawn at the 50% probability level. Hydrogen atoms and non-coordinated solvent molecules are omitted for clarity.

μ,η^1-acetate bridge and a η^1-coordinating acetate ligand completing the coordination sphere of the hydrazide-bound metal center. The metal centers are 324 pm apart with angles of 103° at the phenolate and 102° at the acetate bridge. The heterobimetallic character of **NiZn** is confirmed by the isotope pattern of the $m/z = 685$ signal in the ESI mass spectrum of a solution of **NiZn** in acetonitrile, which is in excellent agreement with the calculated pattern of a $[NiZn(bpampbh)(OAc)]^+$ ion (see below and Figure S2 in the Supporting Information).

The assignment of the metal ions in the crystal structure of **NiZn** is possible by comparing the molecular structures of **ZnZn**, **NiNi**, and **NiZn** (for comparison of the bond angles see Tables S3 and S4 in the Supporting Information). The three complexes have been synthesized in the same way and crystallized under comparable conditions. Consequently, significant structural differences must be related to the presence of different metal ions in the compartments of the supporting unsymmetric ligand. As can be clearly seen in Figure 4, the most striking structural feature that varies within the present complex series is the coordination number of the hydrazide-bound metal atom. The hydrazide compartment in **NiZn** resembles quite well the corresponding binding site in **ZnZn**, with the same coordination environment and distorted geometry ($\tau = 0.31$, as compared to $\tau = 0.35$ for **ZnZn**), whereas the situation in the hydrazide compartment of the homobimetallic nickel complex **NiNi** with its octahedrally coordinated Ni1 atom is quite different. Therefore, the similarities between the zinc-containing complexes on one hand and the differences between the nickel-containing complexes on the other, with regard to the structural features of the hydrazide compartments, strongly indicates that the hydrazide-bound metal center in **NiZn** is a zinc ion.

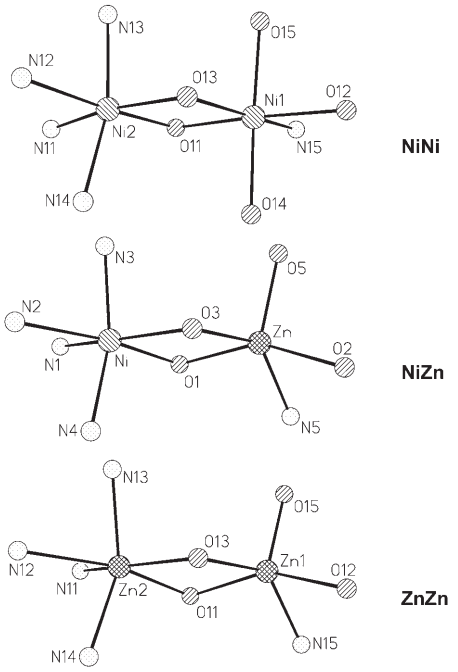

Figure 4. Comparison of the coordination spheres of **NiNi**, **ZnZn**, and **NiZn**.

The coordination environment in the amine compartments of **ZnZn**, **NiNi**, and **NiZn** does not vary to the same extent as that in the hydrazide compartments. The metal centers in all complexes show a distorted octahedral coordination geometry, which is clearly to be ascribed to the rigid preorganized spacial arrangement of the donor atoms of the Schiff-base ligand. This leaves only one predetermined position for the external bridging ligand (acetate for **ZnZn** and **NiZn** and H_2O for **NiNi**). Nevertheless, the distortion from octahedral geometry observed for the amine compartment of **NiZn** with *trans* angles ranging from 158 to 170° is in accordance with the distortion found for **NiNi** and is significantly decreased as compared to the situation in the **ZnZn** complex. Additionally, the bond lengths of the amine-bound metal ions in **NiZn** differ at most by 6 pm from the corresponding values of **NiNi**, whereas the bond lengths observed for **ZnZn** are elongated considerably with the exception of the bond towards the external bridging acetate (Zn2−O13), which is shorter. This exception is consistent with the fact that for an anionic bridging ligand shorter bond lengths can be expected, which is evident from the comparison of relevant bond lengths in **NiNi** (Ni1−O13 210 pm) as well as **ZnZn** (Zn1−O13 205 pm) and **NiZn** (Zn−O3 204 pm), with the first being considerably elongated. To conclude this structural comparison, the metal centers of the heterobimetallic complex **NiZn** can be unambiguously identified as the nickel ion in the amine compartment and the zinc ion in the hydrazide compartment.

The azide-bridged nickel(II) complex **NiNi(N_3)** was obtained by crystallization from the acetonitrile reaction solution. Unfortunately, the quality of the X-ray diffraction data is poor (see Table S5 in the Supporting Information) and only allows the determination of the structural motif (see Figure 5), which is consistent with a $[Ni_2(bpampbh)(\mu,\eta^1\text{-}N_3)]^+$ ion present as its perchlorate salt. An important difference of the molecular structure of **NiNi(N_3)** as compared to the water-bridged homobimetallic nickel complex **NiNi** is the replacement of the bridging water molecule by a μ,η^1-coordinating azide ion. Moreover, in contrast to **NiNi** the diffraction data does not provide any evidence for the presence of apical ligands at the nickel ion residing in the hydrazide compartment of **NiNi(N_3)**. This is corroborated by the fact that the conjugated aromatic plane of the hydrazide compartment together with the bridging phenolate takes part in an extended π-stacking between adjacent homobimetallic cations, with a distance of about 360 pm between the aromatic planes. The absence of additional apical ligands and, therefore, the planarity of the hydrazide-bound nickel ion, is confirmed by elemental analysis, electronic spectroscopy, and SQUID measurements and represents an important structural feature of this compound, as will be discussed later in more detail.

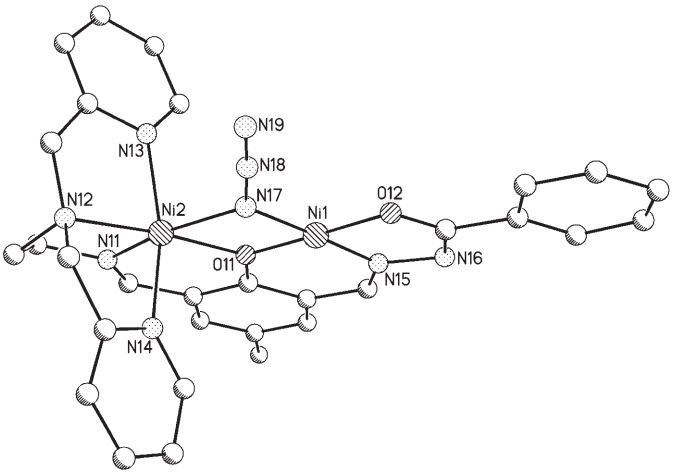

Figure 5. Structural motif of the complex cation $[Ni_2(bpampbh)(\mu,\eta^1\text{-}N_3)]^+$ of **NiNi(N_3)**.

Attempts to generate higher quality crystallographic data by recrystallization of **NiNi(N_3)** in methanol yields the azide-bridged methanol adduct **NiNi(N_3)(MeOH)$_2$**. Its crystal structure reveals one $[Ni_2(bpampbh)(\mu,\eta^1\text{-}N_3)(MeOH)_2]^+$ ion per asymmetric unit with the anions (perchlorate and azide) being located on special positions. The molecular structure of the cation is depicted in Figure 6 and selected bond lengths are given in Table 1. In contrast to complex **NiNi(N_3)**, two apical positions of the hydrazide-bound nickel ion of **NiNi(N_3)(MeOH)$_2$** are occupied by methanol molecules. This results in $[O_4N_2]$ and $[ON_5]$ donor sets for the hydrazide and amine pocket, respectively, both exhibit octahedral geometry with the stronger distortion observed for the nitrogen-rich environment of the amine pocket.

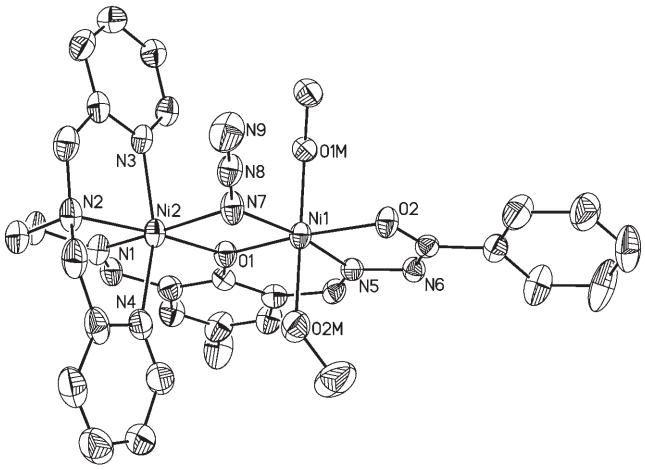

Figure 6. Molecular structure of the complex cation $[Ni_2(bpampbh)(\mu,\eta^1\text{-}N_3)(MeOH)_2]^+$ of **NiNi(N$_3$)(MeOH)$_2$**. Thermal ellipsoids are drawn at the 50% probability level. Hydrogen atoms, non-coordinated solvent molecules, and anions are omitted for clarity.

Comparing the two homobimetallic nickel complexes **NiNi** and **NiNi(N$_3$)(MeOH)$_2$**, the overall structures of both compounds are highly similar. This is clear from the small differences in the corresponding bond lengths (Table 1), which differ at most by 4 pm. In addition, the metal-metal distance of 311 pm in **NiNi(N$_3$)(MeOH)$_2$** as well as the bridge angles of 100 (Ni1–O1–Ni2) and 96° (Ni1–N7–Ni2) are in excellent agreement with the corresponding values of **NiNi**.

Physical properties

Electronic spectra: The visible range of the electronic spectra of solutions of the three nickel-containing complexes in acetonitrile is illustrated in Figure 7 (complete spectra of all complexes are presented in the Supporting Information, data are listed in the Experimental Section). As a common feature of the spectra of **NiZn**, **NiNi**, and **NiNi(N$_3$)** a broad absorption band appears around 940 nm (905 nm for **NiNi(N$_3$)**), attributed to a $^3A_{2g}\rightarrow{}^3T_{2g}$ transition of a high-spin nickel(II) chromophore in an octahedral field.[22] A high-energy shoulder of this absorption band in the range of 800–830 nm is observed in all spectra (most distinct in case of **NiNi(N$_3$)**), suggesting a significant distortion from octahedral symmetry.[23,24] This is in good agreement with the crystallographically determined distortion of the coordination geometry in the amine compartments of all present complexes, and indicates that a considerable contribution of zero-field splitting (ZFS) has to be taken into account in order to interpret the magnetic behavior of the present complexes. At shorter wavelengths of the visible range, the spectra of **NiZn** and **NiNi** show a weak absorption band (merely a broad shoulder in the case of **NiNi**) around $\lambda = 560$ nm that can be assigned to the $^3A_{2g}\rightarrow{}^3T_{1g}(F)$ transition of an octahedral nickel(II) center. In contrast to the pentadentate amine compartment of H_2bpampbh that strongly favors an octahedral geometry, a dissociation equilibrium can be expected in solution for the external apical ligands of a hydrazide-bound metal ion. Two ligand field transitions should be observable for a square-planar low-spin nickel(II) chromophore in the high energy range of the visible spectrum, i.e., the $^1A_{1g}\rightarrow{}^1T_{2g}$ and $^1A_{1g}\rightarrow{}^1B_{1g}$ transition. Therefore, the broadening of the $\lambda = 560$ nm absorption band in the spectrum of **NiNi** indicates the presence of a small amount of a planar species in solution.[22,25]

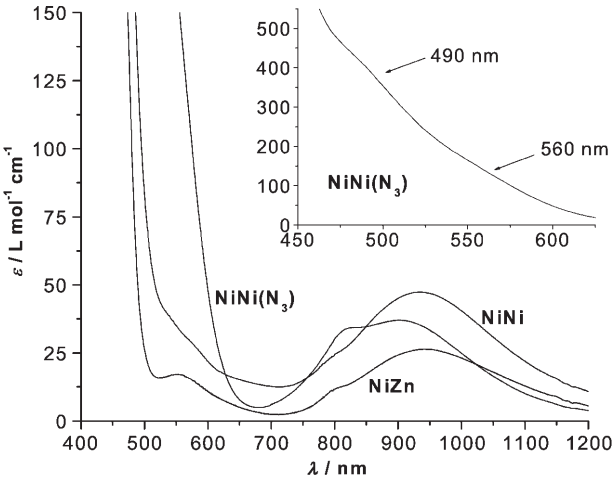

Figure 7. Electronic spectra of complexes **NiZn**, **NiNi**, and **NiNi(N$_3$)** at 20°C in acetonitrile (2×10^{-3} M).

In the electronic spectrum of **NiNi(N$_3$)**, the absorption rapidly increases from about $\lambda = 650$ nm towards shorter wavelengths revealing weak shoulders around $\lambda = 560$ and 490 nm, again indicating the presence of a nickel(II) center with planar geometry. The comparably large intensity of the absorption in this spectral range clearly suggests a rather high concentration of such a planar species in solution and is in good agreement with the assumption of a square-planar coordination geometry of the hydrazide-bound nickel ion in **NiNi(N$_3$)**.

Magnetic properties: The magnetic properties of all nickel-containing complexes were determined by magnetic susceptibility measurements of microcrystalline samples with a SQUID magnetometer as a function of temperature in the range from $T = 2$ to 300 K. The χ_M and $\chi_M T$ plots of the obtained data for complexes **NiNi** and **NiZn** are given in Figure 8. The heterodinuclear complex **NiZn** and the homodinuclear compound **NiNi(N$_3$)** (see Figure S4 in the Supporting Information) exhibit a very similar temperature behavior with essentially invariant $\chi_M T$ curves at $\chi_M T = 1.10\ cm^3 K mol^{-1}$ ($1.33\ cm^3 K mol^{-1}$ for **NiNi(N$_3$)**) from $T = 300$ down to 20 K (15 K for **NiNi(N$_3$)**). This is in agreement with the spin-only value of $\chi_M T = 1.00\ cm^3 K mol^{-1}$ for a single $S = 1$ center,[26] as can be expected for an isolated nickel(II) ion in an octahedral ligand field. Therefore, **NiNi(N$_3$)** magnetically behaves like a mononuclear high-spin nickel(II) compound, with the hydrazide-bound nickel ion in a low-spin configuration ($S = 0$), which is consistent

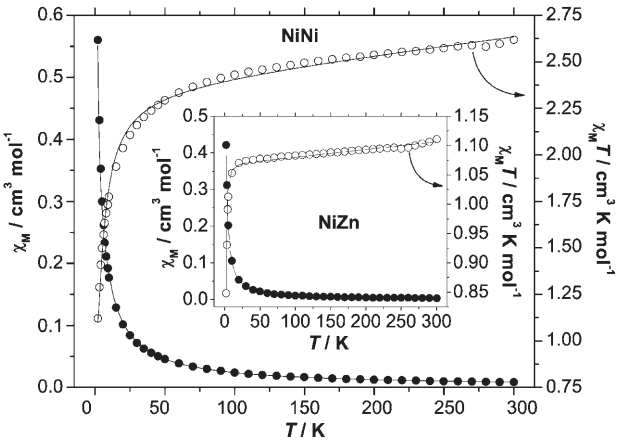

Figure 8. Plots of χ_M (●) and $\chi_M T$ (○) vs. T for complexes **NiNi** and **NiZn** (inset) at an applied field of 5000 Oe. The corresponding fit functions are drawn as solid lines (see text for parameters).

with a planar coordination geometry as indicated by the crystallographic data (see Figure 5). Below $T=20$ K (15 K for **NiNi(N$_3$)**) the $\chi_M T$ values quickly decrease to a value of $\chi_M T=0.85$ cm^3 K mol^{-1} ($\chi_M T=1.11$ cm^3 K mol^{-1} for **NiNi(N$_3$)**) at $T=2$ K, thus indicating a significant zero-field splitting (ZFS). Such a strong magnetic anisotropy is consistent with the electronic spectral data and the molecular structures of all presented nickel-containing complexes as well as the fact that no signal could be detected in the X-band EPR spectra for any of the reported compounds. Assuming axially distorted octahedral symmetry, the energy states of an uncoupled system are obtained by using the Hamiltonian $H=D[S_z^2-{}^1/_3S(S+1)]$. In case of a d^8 system the application of the van Vleck equation leads to the susceptibility expression given in Equation (1) with $A=-D/kT$.

$$\chi_M=\frac{2Ng^2\beta^2}{3kT}\frac{\exp A}{1+2\exp A}+\frac{4Ng^2\beta^2}{3D}\frac{1-\exp A}{1+2\exp A}+\mathrm{TIP} \qquad (1)$$

A fit of the susceptibility data of **NiZn** and **NiNi(N$_3$)** according to Equation (1) yields the parameters $D=2.9\pm0.1$ cm^{-1}, $g=2.07\pm0.01$, and TIP$=1.3\pm0.1$ cm^3 mol^{-1} for **NiZn** and $D=2.2\pm0.1$ cm^{-1}, $g=2.26\pm0.01$, and TIP$=2.0\pm0.1$ cm^3 mol^{-1} for **NiNi(N$_3$)**. Both values of the axial ZFS parameter D are very similar, as can be expected considering the highly related coordination environments of the paramagnetic centers in both complexes. It should be noted here, that variations of χT are in general not very sensitive to the sign of D and, therefore, it is not possible to unambiguously determine the sign of D from magnetic susceptibility data derived from powder measurements.[26]

The $\chi_M T$ curve of the homobimetallic complex **NiNi** (see Figure 8) also appears to be almost invariant over a wide temperature range, but at an overall higher $\chi_M T$ value of about $\chi_M T=2.5$ cm^3 K mol^{-1}. This is in agreement with the spin-only value for a dinuclear complex with two $S=1$ centers,[26] as is expected for molecules containing two nickel(II) ions with octahedral geometries. In contrast to **NiZn** and **NiNi(N$_3$)**, the $\chi_M T$ values of complex **NiNi** gradually decrease over the whole measured temperature range which becomes more pronounced upon lowering the temperature leading to a value of $\chi_M T=1.12$ cm^3 K mol^{-1} at $T=2$ K, which is indicative for a weak antiferromagnetic coupling in addition to the expected ZFS. Especially in cases of weak exchange interactions the ZFS should be taken into account in order to reliably determine the exchange parameter J.[27] This has recently been done for a dinuclear nickel(II) complex.[28] Utilizing the Hamiltonian $H=-JS_1S_2+D[S_z^2-{}^1/_3S(S+1)]$, the van Vleck equation leads to the expression given in Equation (2) for the molar magnetic susceptibility with the following abbreviations: $K=(2J-2D)/kT$, $L=(2J+D)/kT$, $M=(2J+2D)/kT$, $N=-(J+{}^1/_3D)/kT$, and $O=-(J-{}^2/_3D)/kT$.

$$\chi_M=\frac{Ng^2\beta^2}{3kT}\cdot\frac{24\exp K+6\exp L+6\exp N}{2\exp K+2\exp L+\exp M+2\exp N+\exp O+1}+\mathrm{TIP} \qquad (2)$$

Assuming an effective g parameter for both nickel ions, a fit of the susceptibility data of **NiNi** according to Equation (2) results in the parameters $J=-1.4\pm0.4$ cm^{-1}, $D=0.8\pm0.4$ cm^{-1}, $g=2.18\pm0.01$, and TIP$=9.3\pm0.1$ cm^3 mol^{-1}. The negative J value confirms the presence of a weak antiferromagnetic interaction in **NiNi**. Regarding the asymmetry of the complex, the obtained D represents an effective parameter resulting from contributions of two local anisotropies, and therefore it cannot be directly compared to the corresponding values of **NiZn** and **NiNi(N$_3$)**. Nevertheless, the non-zero value of D confirms the assumption of a significant ZFS contribution in **NiNi**.

Electrochemistry: The different coordination environments provided by the two binding compartments of the H_2bpampbh ligand should strongly effect the redox properties of the metal center residing in the respective compartment. The electrochemical differences become evident from a comparison of complexes **NiZn** and **NiNi**. Both systems do not show any oxidation process within the accessible potential range. In contrast, a reduction process is observed in the cyclic voltammogram of the homodinuclear nickel complex **NiNi**, that becomes more resolved at higher scan rates upon which it splits into two distinct peaks (Figure 9), whereas the cyclic voltammogram of the heterobimetallic complex **NiZn** lacks a corresponding peak. Accordingly, the electrode processes observed in the cyclic voltammogram of **NiNi** can be exclusively ascribed to the hydrazide-bound nickel ion. The appearance of two reduction peaks indicates the presence of an adduct formation equilibrium between species of planar and octahedral coordination geometry of the hydrazide-bound nickel(II) ion,[29] probably with acetate ions (present in the crystal structure of **NiNi**) acting as Lewis base. The first peak at -1.58 V corresponds to the reduction of the planar species, whereas the second peak to-

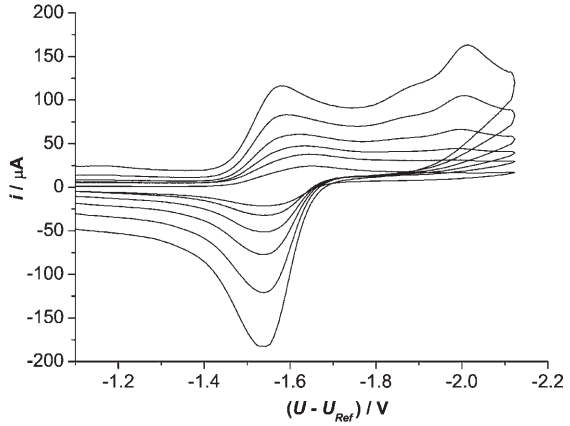

Figure 9. Cyclic voltammogram of a solution of **NiNi** in acetonitrile (1 mM) at scan rates of 2, 5, 10, 20, 40, 77 $V s^{-1}$ (from bottom to top).

wards more negative potential (around −2.0 V) marks the reduction of the octahedral species. The reduction is accompanied by a significant decrease of Lewis acidity, and consequently the backward scan reveals only one peak associated with the oxidation of the planar nickel(I) species. Therefore, the first reduction peak and the reoxidation peak mark a reversible nickel(II)/nickel(I) couple centered around −1.54 V.

Chemical reactivity

Metal exchange reaction: The present complex series shows that both compartments of H_2bpampbh are suitable for binding nickel(II) as well as zinc(II) ions. As could be demonstrated with complex **NiZn**, an equimolar mixture of ligand with both sorts of ions, nickel(II) and zinc(II), results in the selective binding of nickel(II) ions to the amine compartment, whereas the zinc(II) ions are placed in the hydrazide compartment. No homobimetallic side products were observed. This binding selectivity of the ligand compartments led us to the question whether a metal exchange reaction would occur upon mixing solutions of the homobimetallic complexes **ZnZn** and **NiNi**. In order to elucidate this question, we heated a solution of equimolar amounts of **ZnZn** and **NiNi** in methanol under reflux and examined the resulting composition of complex species by means of electrospray ionization (ESI) mass spectrometry (Figure 10). Interestingly, already after 1 h reaction time the predominant species in the reaction mixture could be identified as the heterobimetallic μ-methanolato-bridged [NiZn(bpampbh)(μ-OMe)]$^+$ ion ($m/z = 657$), and only small amounts of the corresponding homobimetallic nickel and zinc species could be detected. Therefore, an efficient metal exchange reaction occurs between the homobimetallic compounds. No significant changes were observed after extending the reaction time to 5 h, indicating an exchange equilibrium between homo- and heterobimetallic compounds with the heterobimetallic species being thermodynamically favored. This is in agreement with the fact that no homobimetallic side products have been observed in the synthesis of **NiZn**, in which nickel(II) and zinc(II) acetate are reacted simultaneously

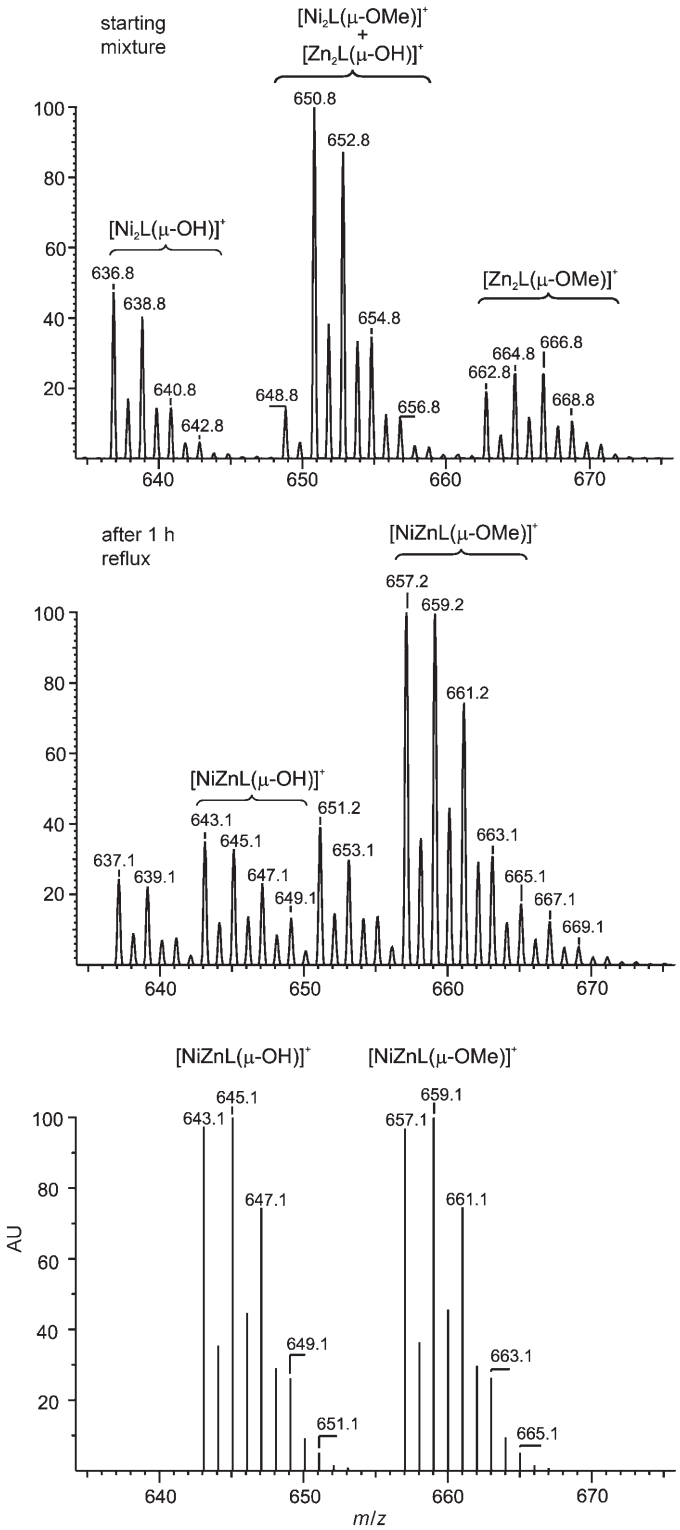

Figure 10. Metal exchange reaction in an equimolar solution of **ZnZn** and **NiNi** in methanol, monitored by ESI mass spectrometry (L = bpampbh^{2-}). ESI mass spectra of the reaction mixture were recorded before (top) and after 1 h reaction time under reflux (middle). For comparison, the calculated isotope patterns (bottom) of the [NiZn(bpampbh)(μ-OH)]$^+$ ($C_{30}H_{29}N_6O_3NiZn$) and [NiZn(bpampbh)(μ-OMe)]$^+$ ($C_{31}H_{31}N_6O_3NiZn$) ions are shown (isotope patterns of the corresponding homobimetallic ions are illustrated in Figure S3 in the Supporting Information).

with the ligand solution. Accordingly, the formation of **NiZn** represents a highly directed process, driven by the chemically distinct ligand compartments matching the different coordination preferences of the metal ions.

Solutions in protic and aprotic solvents: Compounds **ZnZn**, **NiNi**, and **NiZn** show good solubility in various polar and protic solvents, including water and chloroform, whereas **NiNi(N$_3$)** is soluble in acetonitrile, but only moderately soluble in protic solvents and essentially insoluble in non-coordinating solvents. The ESI mass spectra of the complex solutions are dominated by signals that can be assigned to $[MM(bpampbh)(\mu\text{-}X)]^+$ ions (Scheme 3), in which the nature of the bridging X^- depends on the solvent and the anions present in the solid-state structure of the complexes (mass spectrometric data of solutions in different solvents are listed in the Experimental Section and the Supporting Information). In acetonitrile, the bridging X^- ligand of the predominant species corresponds to the bridge found in the respective crystal structure. In contrast, upon dissolving the complexes in the protic solvents methanol or water, the bridging units are replaced by the respective solvent-derived anions, and the predominant ESI-MS signals can be assigned to $[MM(bpampbh)(\mu\text{-}OMe)]^+$ or $[MM(bpampbh)(\mu\text{-}OH)]^+$ ions, respectively. Additionally, in case of a solution of **ZnZn** in methanol/water, a significant signal of the mononuclear cation $[Zn(Hbpampbh)]^+$ was detected, indicating a partial dissociation of the complex under the experimental conditions in solution. Only trace amounts of corresponding mononuclear species were observed for the nickel-containing complexes, indicating a stronger binding of nickel. Nevertheless, no dissociation is evident from the NMR spectrum of a solution of **ZnZn** in methanol. Therefore, we can conclude from our solution studies that the present complexes are stable in aprotic as well as protic solvents under ambient conditions. In particular, no hydrolysis of the ligand occurs even in aqueous solution or refluxing methanol.

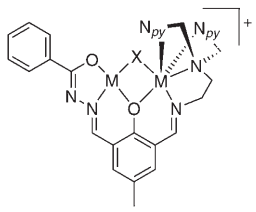

Scheme 3. Formula of the $[MM(bpampbh)(\mu\text{-}X)]^+$ ions found in ESI mass spectra (M = Ni and Zn).

Adduct formation: As an effect of the ligand-induced strong asymmetry of our systems regarding the donor sets, coordination numbers and geometries, the two metal centers in each complex can be expected to show rather different chemical reactivities. The amine compartment with its strongly chelating pentadentate donor set results in a rather rigid coordination environment, whereas the tridentate hydrazide compartment leaves three binding positions potentially accessible for external donor functionalities. As is evident from the electrochemical properties of **NiNi** (vide supra), the hydrazide-bound nickel center can be expected to possess a significant Lewis acidity in its divalent oxidation state, resulting in the formation of adduct species in presence of suitable donor molecules. In the case of a nickel(II) ion as a Lewis acidic center, the process of adduct formation can be monitored spectrophotometrically, owing to the high sensitivity of the nickel(II) spin state towards changes in coordination number and geometry, leading to a low spin $S=0$ state in planar and a high-spin $S=1$ state in octahedral field.[22] Therefore, we carried out photometric titration experiments with solutions of **NiNi(N$_3$)** in acetonitrile. In contrast to **NiNi**, the hydrazide-bound nickel ion in **NiNi(N$_3$)** lacks apical ligands. While the presence of two equivalents of acetate per complex molecule in **NiNi** represents an inherent problem for any titration with donor functionalities, the adduct formation in solutions of **NiNi(N$_3$)** is not impaired by coordination equilibria introduced by competing coordinating anions. As is evident from the mass spectrometric results, the $[Ni_2(bpampbh)(\mu\text{-}N_3)]^+$ ion is the dominant species in solutions of **NiNi(N$_3$)** in acetonitrile, possibly weakly ligated by solvent molecules. This makes **NiNi(N$_3$)** an appropriate candidate for quantitative reactivity studies regarding the adduct formation of the $[MM(bpampbh)(\mu\text{-}X)]^+$ motif towards donor molecules.

The titrations were carried out by using acetate as anionic and pyridine as neutral coligand (Figure 11). The same general spectral changes occur in both titrations, i.e., a decrease in absorbance between $\lambda=480$ and 615 nm with a larger variation in case of acetate addition, which is in accordance to a decreasing concentration of four-coordinate species in both systems (vide supra). The spectral curves pass through well-defined isosbestic points up to an addition of one equivalent of acetate or pyridine, to suggest an equilibrium between planar starting complex and five-coordinate adduct. Upon further titration, the spectral changes indicate the formation of a second reaction product, presumably a six-coordinate species. Accordingly, we can formulate a two-step equilibrium in Equation (3) for the adduct formation of **NiNi(N$_3$)**, with the $bpampbh^{2-}$ anion denoted as L and B representing the added base.

$$[Ni_2L(\mu\text{-}N_3)]^+ + B^{n-} \overset{K_1}{\rightleftharpoons} [Ni_2L(\mu\text{-}N_3)(B)]^{(1-n)+} + B^{n-} \overset{K_2}{\rightleftharpoons} [Ni_2L(\mu\text{-}N_3)(B)_2]^{(1-2n)+} \quad (3)$$

A fit of the spectral data by means of the program SpecReg[30] results in $K_1=400\pm100\,L\,mol^{-1}$ and $K_2=70\pm10\,L\,mol^{-1}$ for the pyridine system and $K_1=(4.4\pm0.2)\times10^4\,L\,mol^{-1}$ and $K_2=900\pm100\,L\,mol^{-1}$ for the acetate system. The relatively large uncertainties in the fit of the pyridine system are a consequence of the only small spectral changes during the titration procedure. However, the results clearly show that the $[Ni_2(bpampbh)(\mu\text{-}N_3)]^+$ ion has a strong affinity towards Lewis bases, especially to anionic species, as is expected for a positively charged planar nickel(II) complex. Interestingly, the equilibrium constant of the second addition step in both systems is about an order of magnitude smaller than K_1, contradicting the common observation that the diadduct of nickel(II) Schiff-base com-

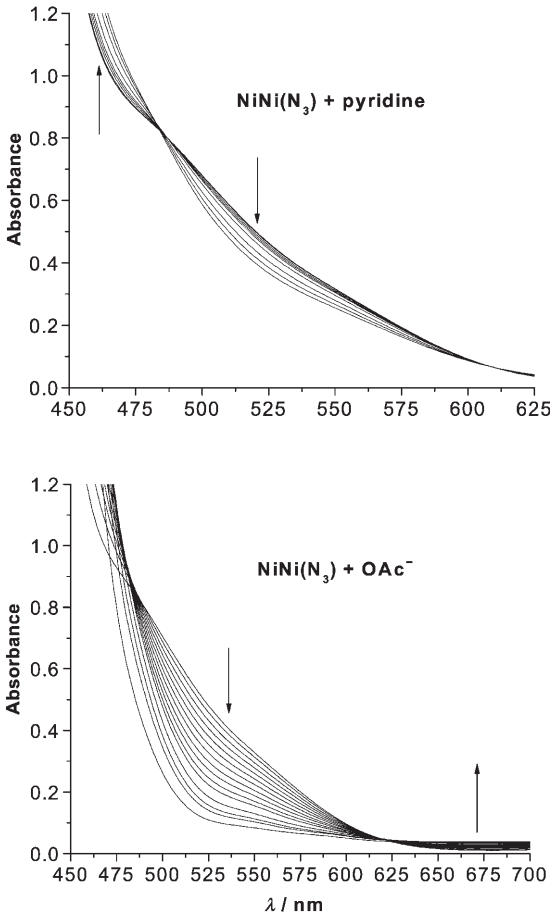

Figure 11. Photometric titration of **NiNi(N_3)** in acetonitrile (2 mM) at 20 °C. Top: Addition of pyridine (0, 0.1, 0.3, 0.5, 0.7, 1.2, 2.2, 3.2, and 4.2 equivalents); Bottom: Addition of tetra-*n*-butylammonium acetate (0, 0.1, 0.2, 0.3, 0.4, 0.5, 0.6, 0.7, 0.8, 0.9, 1.0, 1.2, 1.4, 1.6, 2.1 equivalents); Absorbance data were corrected for dilution effects.

plexes is the generally favored and more stable species.[31] A possible explanation for this unexpected behavior is that, instead of an adduct formation of a planar nickel(II), a ligand exchange reaction of an octahedral solvent adduct is observed. On the other hand, the electronic spectrum of **NiNi(N_3)** clearly indicates the presence of a planar nickel(II) chromophore in acetonitrile. However, the donating character of acetonitrile seems to play a significant role in the present system. This problem could be circumvented by usage of a non-coordinating solvent for the titration experiment. Unfortunately, **NiNi(N_3)** is only poorly soluble in any such solvent. Nevertheless, the titrations unambiguously show the high reactivity of the hydrazide-bound metal ion in H_2bpampbh-based complexes towards Lewis bases, especially anions. The diadduct is formed, but the equilibrium constant of the second addition is strongly reduced compared to the corresponding constant of the first addition step.

SOD-like reactivity: The observed strong Lewis acidity of the hydrazide-bound metal center in our H_2bpampbh complexes led us to the question whether we could observe any reactivity towards Lewis bases of biological relevance. With respect to the importance of the nickel-dependent superoxide dismutase (NiSOD) in prokaryotic species[32,33] we were interested in examining the ability of our system to react with superoxide radicals. The reactivity tests were carried out with **NiNi** for its good water solubility and the potentially reactive nickel center in the hydrazide compartment. The xanthine/xanthine oxidase system was used for the in situ generation of superoxide in solution, the time-dependent radical concentration was indirectly monitored by following the reduction of nitro blue tetrazolium (NBT) spectrophotometrically.[34,35] As can be seen in Figure 12, the NBT reduction is significantly inhibited upon addition of **NiNi**. The reaction shows saturation behavior, reaching 100% inhibition at complex concentrations of about 150 μM. The IC_{50} concentration of **NiNi**, leading to 50% inhibition of the NBT reduction, is about 60 μM (corresponding to an activity of 0.05 U/mg), which is two orders of magnitude higher compared to reported synthetic coordination compounds of high activity.[36] Accordingly, the SOD-like reactivity of **NiNi** is weak, but nevertheless significant, as no inhibition of NBT reduction was observed for free nickel(II) acetate. Therefore we can exclude that the found activity is caused by small amounts of nickel ions set free from the **NiNi** complex by dissociation processes. Additionally, the formation of uric acid by the xanthine/xanthine oxidase system was not affected by the complex and therefore the observed inhibition is not the result of direct interaction with the enzyme.

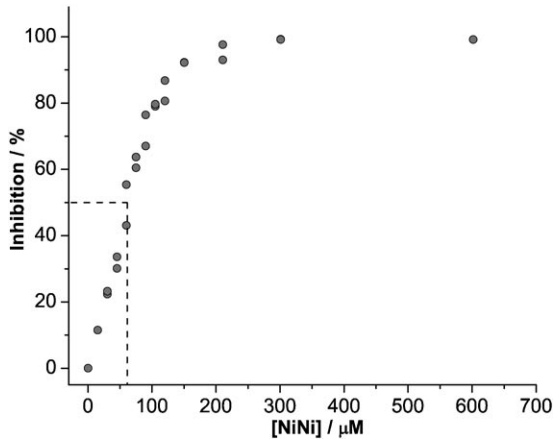

Figure 12. Percentage of inhibition of NBT reduction by complex **NiNi**, plotted as a function of **NiNi** concentration. Superoxide radicals were generated with the xanthine/xanthine oxidase system. The inhibition for each complex concentration was doubly determined.

Conclusion

In this study, we synthesized the new unsymmetric "end-off" double Schiff-base ligand H_2bpampbh by sequential reaction of an aromatic dicarbonyl bridging unit and two primary amines, demonstrating the versatility of this straight-forward

synthetic strategy towards unsymmetric ligand systems, that has been recently developed by us.[21] The ligand molecule provides two entirely different binding compartments, which are both suitable for accommodating either zinc(II) or nickel(II) ions, as we have shown by way of the homodinuclear complexes **ZnZn** and **NiNi**. In case of simultaneous presence of both metal ions the formation of the heterodinuclear complex **NiZn** is observed. This process is highly directed by the different coordination requirements of the metal ions and the distinct chemical environments of the ligand compartments, resulting in a hydrazide-bound zinc, whereas nickel is selectively placed in the amine compartment of the H_2bpampbh ligand.

An interesting feature of our system are two variable binding positions at the hydrazide-bound metal center that are accessible for external donor molecules. The strong Lewis acidity of the hydrazide-bound metal site, quantified for the homobimetallic nickel system by spectrophotometric titrations, makes H_2bpampbh-based complex compounds suitable candidates for activity tests in catalytic reactions. In this study we demonstrated that the homobimetallic complex **NiNi** shows low but significant SOD-like activity in inhibiting the reduction of NBT by superoxide radicals. Considering the water solubility of the present complexes and the importance of nickel and zinc in hydrolytically active enzymes, the examination of our system regarding urease and phosphatase activity seems promising and is subject of our ongoing work.

Furthermore, while the main goal of the present work was to confirm the versatility and high potential of our synthetic route towards unsymmetric ligand and complex systems, our future efforts will be focused on the directed generation of unsymmetric coordination compounds with closer relation to biological systems, thus promising and interesting bioanalog properties. As we could demonstrate in this paper, our synthetic approach provides an appropriate tool for this purpose.

Experimental Section

Physical measurements: The NMR spectra were recorded on a Bruker Avance 400 MHz spectrometer. IR spectra were measured on a Bruker IFS55/Equinox spectrometer. For UV/Vis solution spectra a Varian Cary 5000 UV/Vis/NIR spectrophotometer equipped with a dual cell peltier accessory was used. Mass spectra were recorded on a MAT95XL Finnigan instrument. Elemental analyses were acquired by use of a LECO CHN/932 and a VARIO EL III elemental analyzer. Cyclic voltammetry measurements have been performed by means of a three electrode technique by using a home built computer controlled instrument (for details see[37]). The experiments were performed in solutions of tetra-*n*-butylammonium perchlorate (0.25 M) in acetonitrile under a blanket of solvent saturated with argon. Ag/AgCl was used as reference electrode in a solution of tetra-*n*-butylammonium chloride (0.25 M) in acetonitrile. The reported potentials are referenced with respect to the ferrocenium/ferrocene couple, which was recorded at the end of each experiment. The working electrode was a hanging mercury drop ($m_{Hg-drop} \approx 4$ mg) generated by a CGME instrument (Bioanalytical Systems, West Lafayette, USA). Magnetic susceptibilities were measured with a Quantum Design MPMSR-5S-SQUID magnetometer in the range from $T = 2$ to 300 K at magnetic fields of 5000 Oe. Diamagnetic corrections were estimated according to Pascal's constants.

Syntheses: Proligand Hbpahmb was synthesized as previously reported.[21] All other chemicals and solvents are commercially available and were used without further purification.

Benzoic acid [1-(3-{[2-(bispyridin-2-ylmethylamino)ethylimino]methyl}-2-hydroxy-5-methylphenyl)methylidene]hydrazide (H_2bpampbh): A solution of Hbpahmb in methanol was treated with one equivalent benzoic acid hydrazide dissolved in methanol, accompanied by a color change of the solution from yellow to bright red. After two hours of stirring at room temperature, the solvent was removed in vacuo. The crude product was purified by size exclusion chromatography with Sephadex LH-20 to remove small quantities of the symmetric side products, and H_2bpampbh was obtained as an analytically pure, highly viscous red oil. Yield: 82%. ^{1}H NMR (DMSO, 400 MHz): $\delta = 2.29$ (s, 3H; CH_3), 2.81 (t, $^3J = 5.80$ Hz, 2H; N–CH_2), 3.76 (t, $^3J = 5.88$ Hz, 2H; =N–CH_2), 3.83 (s, 4H; N–CH_2–py), 7.21 (m, 2H; CH_{py}), 7.26 (m, 1H; CH_{Ph}), 7.45–7.68 (m, 7H; 4CH_{py} and 3CH_{Ph}), 7.77 (m, 1H; CH_{Ph}), 7.94 (m, 2H; CH_{Ph}), 8.46 (m, 2H; CH_{py}), 8.50 (s, 1H; HC=N), 8.84 (s, 1H; HC=N–N), 11.87 (s, 1H; NH), 14.29 ppm (s, 1H; OH); ^{13}C NMR (DMSO, 100 MHz): $\delta = 20.4$ (CH_3), 54.3 (N–CH_2), 55.1 (=N–CH_2), 60.1 (N–CH_2–py), 118.9 (C_{Ph}), 120.6 (C_{Ph}), 122.6 (C_{py}), 123.0 (C_{py}), 126.5, 128.1, 128.9, 129.8, 132.1, 133.9, 134.3 (all C_{Ph}), 136.9 (C_{py}), 143.7 (C=N–N), 149.2 (C_{py}), 159.6 (C_{py}), 160.9 (C=N), 163.4 (C–OH), 166.7 ppm (C=O); IR(KBr): $\tilde{\nu} = 3215$ (N–H), 1636 cm^{-1} (Amide I and C=N); MS (micro-ESI in methanol): m/z: 529 (100%, $[H_2bpampbh + Na]^+$); elemental analysis calcd (%) for $H_2bpampbh \cdot H_2O$, $C_{30}H_{32}N_6O_3$, (524.62): C 68.68, H 6.15, N 16.02; found: C 68.44, H 6.29, N 16.77.

[Zn_2(bpampbh)(μ,η^1-OAc)(η^1-OAc)] (ZnZn): The ligand H_2bpampbh (200 μmol) and triethylamine (2 equiv) were dissolved in acetonitrile (20 mL). Solid $Zn(OAc)_2 \cdot 2H_2O$ (2 equiv) was added, and the resulting mixture was stirred for 2 h at room temperature. The metal salt dissolved completely upon complexation and the color of the reaction mixture turned from yellow-red to bright yellow. Single crystals suitable for X-ray crystallography were obtained after a few days at −20 °C. After reduction of the solution volume, a second crystalline sample could be obtained. Overall yield: 61%. ^{1}H NMR (MeOD, 400 MHz): $\delta = 1.95$ (s, 6H; CH_3 acetate), 2.27 (s, 3H; CH_3), 2.86 (t, $^3J = 5.20$ Hz, 2H; CH_2–N=), 3.06 (t, $^3J = 5.18$ Hz, 2H; CH_2–N), 4.37 (d, $^2J = 16.01$ Hz, 2H; 1H of each CH_2–py), 4.67 (d, $^2J = 16.01$ Hz, 2H; 1H of each CH_2–py), 7.13 (m, 1H), 7.32–7.40 (m, 6H), 7.47 (m, 2H), 7.90 (m, 2H), 8.01 (m, 2H) (all CH_{arom}), 8.10 (s, 1H; HC=N), 8.56 (m, 2H; CH_{arom}), 8.69 ppm (s, 1H; HC=N–N); ^{13}C NMR (MeOD, 100 MHz): $\delta = 19.8$ (CH_3), 23.7 (CH_3 acetate), 56.2 (CH_2–N), 59.8 (CH_2–N=), 62.5 (CH_2–py), 123.7, 124.3, 125.6, 126.5, 128.9, 129.0, 131.6, 136.9, 140.4, 140.9, 141.0, 149.0 (all C_{arom}), 156.2 (C=N–N), 157.0 (C_{arom}), 167.1 (Ph–O), 169.2 (C=N), 173.7 (N=C–O), 179.6 ppm (C=O acetate); IR(KBr): $\tilde{\nu} = 1647$ and 1606 cm^{-1} (C=N and C=N–N=C); UV/Vis (MeCN): λ_{max} (ε) = 292 (13400), 343 (12000), 402 (16700), 415 nm (sh, 16400 M^{-1}cm^{-1}) (see Figure S5 in the Supporting Information); MS (micro-ESI in methanol/acetonitrile): m/z: 651 ($[Zn_2(bpampbh)(OH)]^+$), 665 ($[Zn_2(bpampbh)(OMe)]^+$), 693 (100%, $[Zn_2(bpampbh)(OAc)]^+$); elemental analysis calcd (%) for $[Zn_2(bpampbh)(OAc)_2](H_2O)_3$, $C_{34}H_{40}N_6O_9Zn_2$ (807.5): C 50.57, H 4.99, N 10.41; found: C 50.74, H 4.56, N 10.04.

[Ni_2(bpampbh)(μ-H_2O)(η^1-OAc)(H_2O)](OAc) (NiNi): A solution of the ligand H_2bpampbh (200 μmol) and triethylamine (2 equiv) in acetonitrile (15 mL) was added to a suspension of $Ni(OAc)_2 \cdot 4H_2O$ (2 equiv) in acetonitrile (5 mL). After 2 h stirring at room temperature, the nickel salt was completely dissolved. The volume of the mixture was reduced to 10 mL and the resulting red-brown solution was left at −20 °C. Single crystals suitable for X-ray crystallography were obtained after a few days. A second crop of crystalline material could be isolated by slow evaporation at room temperature after two days. Overall yield: 68%. IR(KBr): $\tilde{\nu} =$ 1650 and 1606 cm^{-1} (C=N and C=N–N=C); UV/Vis (MeCN): $\lambda_{max}(\varepsilon) =$ 307 (15400), 349 (13400), 407 (14000), 570 (sh, 30), 802 (sh, 25), 937 nm (47 M^{-1}cm^{-1}) (see Figure S6 in the Supporting Information); MS (micro-ESI in acetonitrile): m/z: 637 (100%, $[Ni_2(bpampbh)(OH)]^+$), 679 ($[Ni_2(bpampbh)(OAc)]^+$); elemental analysis calcd (%) for

$[Ni_2(bpampbh)(OAc)(H_2O)_2](OAc)(H_2O)_3$, $C_{34}H_{44}N_6O_{11}Ni_2$ (830.13): C 49.19, H 5.34, N 10.12; found: C 49.28, H 5.27, N 10.14.

[NiZn(bpampbh)(μ,η¹-OAc)(η¹-OAc)] (NiZn): A solution of the ligand H_2bpampbh (200 μmol) and triethylamine (2 equiv) in acetonitrile (15 mL) was added to a suspension of $Ni(OAc)_2{\cdot}4H_2O$ (1 equiv) and $Zn(OAc)_2{\cdot}2H_2O$ (1 equiv) in acetonitrile (5 mL). After 2 h stirring at room temperature, the metal salts were completely dissolved. The volume of the mixture was reduced to 10 mL and the resulting brown solution was left at −20 °C. Single crystals suitable for X-ray crystallography were obtained after a few days. Yield: 71 %. IR(KBr): $\tilde{\nu}$ = 1652 and 1606 cm^{-1} (C=N and C=N−N=C); UV/Vis (MeCN): $\lambda_{max}(\varepsilon)$ = 305 (14200), 345 (13200), 404 (16600), 417 (sh, 16200), 552 (17), 798 (sh, 11), 942 nm (26 $M^{-1}cm^{-1}$) (see Figure S7 in the Supporting Information); MS (micro-ESI in acetonitrile): *m*/*z*: 685 (100 %, $[NiZn(bpampbh)(OAc)]^+$); elemental analysis calcd (%) for $[NiZn(bpampbh)(OAc)_2]{\cdot}(H_2O)_{2.5}(HOAc)_{0.5}$, $C_{35}H_{41}N_6O_{9.5}NiZn$ (821.82): C 51.15, H 5.03, N 10.23; found: C 51.32, H 5.05, N 10.29.

CAUTION! *In general, perchlorate salts of metal complexes with organic ligands are potentially explosive. While the present complex has not proved to be shock sensitive, only small quantities should be prepared and great care is recommended.*

$[Ni_2(bpampbh)(\mu,\eta^1\text{-}N_3)]ClO_4$ (NiNi(N_3)): A solution of the ligand H_2bpampbh (200 μmol) and triethylamine (2 equiv) in acetonitrile (15 mL) was reacted with a solution of $Ni(ClO_4)_2{\cdot}6H_2O$ (2 equiv) in acetonitrile (5 mL) at room temperature. After stirring for 10 min, one equivalent of solid NaN_3 was added to the red-brown solution. After further stirring for 2 h, the NaN_3 dissolved completely and **NiNi(N_3)** was obtained as polycrystalline brown solid at −20 °C. Yield: >70 %. Single crystals were isolated by slow evaporation of the reaction solution. Redissolving **NiNi(N_3)** in methanol and subsequent slow evaporation of the solvent resulted in crystallization of the methanol adduct $[Ni_2(bpampbh)(\mu,\eta^1\text{-}N_3)(MeOH)_2](ClO_4)_{0.5}(N_3)_{0.5}$ (**NiNi(N_3)(MeOH)$_2$**). All given analytical data are based on the **NiNi(N_3)** derivative unless otherwise stated. IR(KBr): $\tilde{\nu}$ = 2078 (μ-N_3), 1652 and 1607 (C=N and C=N−N=C), 1095 cm^{-1} (ClO_4); UV/Vis (MeCN): $\lambda_{max}(\varepsilon)$ = 302 (18000), 357 (13000), 413 (11600), 490 (sh, 400), 560 (sh, 140), 828 (34), 905 nm (37 $M^{-1}cm^{-1}$) (see Figure S8 in the Supporting Information); UV/Vis (MeOH): $\lambda_{max}(\varepsilon)$ = 303 (18000), 335 (13300), 395 (sh, 11400), 414 (12100), 540 (43), 885 nm (51 $M^{-1}cm^{-1}$) (see Figure S9 in the Supporting Information); MS (micro-ESI in acetonitrile): *m*/*z*: 662 (100 %, $[Ni_2(bpampbh)(N_3)]^+$); elemental analysis calcd (%) for $[Ni_2(bpampbh)(N_3)](ClO_4)(H_2O)_{0.25}$, $C_{30}H_{28.5}N_9O_{6.25}ClNi_2$ (767.95): C 46.92, H 3.74, N 16.42; found: C 47.02, H 3.64, N 16.48.

Measurements of SOD-like reactivity: Superoxide radical anions were generated using the xanthine/xanthine oxidase system, the time-dependent radical concentration was monitored by following the reduction of nitro blue tetrazolium (NBT) to formazan dye spectrophotometrically at 560 nm.[34,35] All solutions were prepared by using phosphate buffer (50 mM, pH 7.8) as solvent. In a typical experiment, NBT (75 μL, 2.2 mM), xanthine (100 μL, 800 μM), complex solution (100 μL, 0 to 10 mM), and buffer (900 μL) were mixed in a cuvette placed in the spectrophotometer. The reaction was started by adding a solution of xanthine oxidase (500 μL, 52 μg mL^{-1}) and stopped after 120 s. The inhibition of the NBT reduction is calculated according to $I(\%) = (\Delta A_0 - \Delta A_c){\cdot}100/\Delta A_0$, in which ΔA_0 and ΔA_c are the observed absorbance changes in absence or presence of complex, respectively. The experiment was carried out twice for each complex concentration. To evaluate whether the generation of superoxide by xanthine oxidase is affected by direct interactions between the examined complex and the enzyme, the formation rate of uric acid in the system was kinetically followed at 290 nm in absence and presence of **NiNi**.

X-ray crystallographic studies: The intensity data were collected on a Nonius KappaCCD diffractometer using graphite-monochromated $Mo_{K\alpha}$ radiation. Data were corrected for Lorentz and polarization effects, but not for absorption.[38,39,40] Details of data collection and refinement procedure are summarized in Table 2 (Table S5 in the Supporting Information for **NiNi(N_3)**). The structures were solved by direct methods with the program SHELXS-97[41] and refined by full-matrix least squares techniques against F_o^2 with the software package SHELXL-97.[41] All non-hydrogen atoms were refined anisotropically, except the disordered acetate ligands and the acetonitrile and water molecules in **ZnZn** placed on half-occupied positions as well as the non-coordinated solvent molecules and the azide counter ion in **NiNi(N_3)(MeOH)$_2$**. The diffraction data obtained for **NiNi(N_3)** only allowed the determination of the structural motif of the complex cation (for selected structural parameters see Table S6 in the Supporting Information). The residual electron density indicates a disorder problem of one of the ligand-based pyridyl groups, which could not be resolved. Nevertheless, it is important to note that no electron density is found that would indicate the existence of apical ligands of the hydra-

Table 2. Crystal data, data collection, and refinement parameters for compounds **ZnZn**, **NiNi**, **NiZn**, and **NiNi(N_3)(MeOH)$_2$**.

	ZnZn	**NiNi**	**NiZn**	**NiNi(N_3)(MeOH)$_2$**
formula	$C_{35}H_{34.83}N_{6.5}O_{6.17}Zn_2$	$C_{35.5}H_{40.25}N_{6.75}O_{10.5}Ni_2$	$C_{37.3}H_{39.6}N_7O_{7.3}NiZn$	$C_{33}H_{40}N_{10.5}O_{7.5}Cl_{0.5}Ni_2$
M_r [g mol^{-1}]	775.93	851.95	826.84	838.90
T [K]	183(2)	183(2)	183(2)	183(2)
crystal size [mm]	0.5×0.5×0.4	0.6×0.6×0.5	0.6×0.6×0.4	0.5×0.5×0.5
crystal system	triclinic	triclinic	orthorhombic	monoclinic
space group	$P\bar{1}$	$P\bar{1}$	$P2_12_12_1$	$C2/c$
a [pm]	1087.160(10)	1157.45(5)	1538.34(4)	3026.87(9)
b [pm]	1691.81(3)	1757.59(7)	1544.72(3)	2173.87(8)
c [pm]	2826.36(4)	2030.65(5)	1768.36(5)	1413.61(4)
α [°]	82.7480(10)	86.600(2)	90.00	90.00
β [°]	87.5020(10)	75.993(2)	90.00	114.832(2)
γ [°]	85.2740(10)	82.958(2)	90.00	90.00
V [nm^3]	5.13642(13)	3.9760(3)	4.20216(18)	8.4416(5)
Z	6	4	4	8
ρ_{calcd} [g cm^{-3}]	1.505	1.423	1.307	1.320
μ [mm^{-1}]	1.457	1.011	1.072	0.979
θ_{min}, θ_{max} [°]	2.34, 27.49	2.56, 27.47	2.19, 27.47	2.22, 27.49
unique data	23161	17936	9602	9678
data with $I > 2\sigma(I)$	15922	9829	7668	6084
no. of parameters	1344	1040	530	481
ωR_2 (all data, F_o^2)	0.1300	0.1474	0.1435	0.2498
R_1 ($I > 2\sigma(I)$)	0.0510	0.0575	0.0501	0.0733
flack-parameter	–	–	−0.025(14)	–

zide-bound nickel center. The programs XP (SIEMENS Analytical X-ray Instruments) was used for structure representations.

CCDC–654629, 654630, 654631, 654632, and 654633 contain the supplementary crystallographic data for this paper. These data can be obtained free of charge from The Cambridge Crystallographic Data Centre via www.ccdc.cam.ac.uk/data_request/cif.

Acknowledgements

This work was supported by a grant from the Deutsche Forschungsgemeinschaft (SFB 436 "Metal-Mediated Reactions Modeled after Nature") and A. R. gratefully acknowledges the support by a Graduiertenstipendium of the Freistaat Thüringen.

[1] P. Nordlund, H. Eklund, *Curr. Opin. Struct. Biol.* **1995**, *5*, 758–766.
[2] R. H. Holm, P. Kennepohl, E. I. Solomon, *Chem. Rev.* **1996**, *96*, 2239–2314.
[3] D. M. Kurtz, Jr., *J. Biol. Inorg. Chem.* **1997**, *2*, 159–167.
[4] C. Belle, J.-L. Pierre, *Eur. J. Inorg. Chem.* **2003**, 4137–4146.
[5] J. H. Satcher, Jr., M. W. Droege, T. J. R. Weakley, R. T. Taylor, *Inorg. Chem.* **1995**, *34*, 3317–3328.
[6] S. J. Lippard, *Science* **1995**, *268*, 996–997.
[7] R. E. Stenkamp, *Chem. Rev.* **1994**, *94*, 715–726.
[8] N. Mitić, S. J. Smith, A. Neves, L. W. Guddat, L. R. Gahan, G. Schenk, *Chem. Rev.* **2006**, *106*, 3338–3363.
[9] J. A. Tainer, E. D. Getzoff, J. S. Richardson, D. C. Richardson, *Nature* **1983**, *306*, 284–287.
[10] D. Ghosh, S. Mukhopadhyay, S. Samanta, K.-Y. Choi, A. Endo, M. Chaudhury, *Inorg. Chem.* **2003**, *42*, 7189–7199.
[11] Y. Tachi, K. Aita, S. Teramae, F. Tani, Y. Naruta, S. Fukuzumi, S. Itoh, *Inorg. Chem.* **2004**, *43*, 4558–4560.
[12] M. Konrad, S. Wuthe, F. Meyer, E. Kaifer, *Eur. J. Inorg. Chem.* **2001**, 2233–2340.
[13] R. A. Peralta, A. Neves, A. J. Bortoluzzi, A. Casellato, A. dos Anjos, A. Greatti, F. R. Xavier, B. Szpoganicz, *Inorg. Chem.* **2005**, *44*, 7690–7692.
[14] M. F. Anderlund, J. Högblom, W. Shi, P. Huang, L. Eriksson, H. Weihe, S. Styring, B. Åkermark, R. Lomoth, A. Magnuson, *Eur. J. Inorg. Chem.* **2006**, 5033–5047.
[15] D. E. Fenton, *Inorg. Chem. Commun.* **2002**, *5*, 537–547.
[16] D. E. Fenton, *Chem. Soc. Rev.* **1999**, *28*, 159–168.
[17] R. Than, A. A. Feldmann, B. Krebs, *Coord. Chem. Rev.* **1999**, *182*, 211–241.
[18] A. L. Gavrilova, B. Bosnich, *Chem. Rev.* **2004**, *104*, 349–383.
[19] P. A. Vigato, S. Tamburini, *Coord. Chem. Rev.* **2004**, *248*, 1717–2128.
[20] T. Koga, H. Furutachi, T. Nakamura, N. Fukita, M. Ohba, K. Takahashi, H. Ōkawa, *Inorg. Chem.* **1998**, *37*, 989–996.
[21] A. Roth, E. T. Spielberg, W. Plass, *Inorg. Chem.* **2007**, *46*, 4362–4364.
[22] A. B. P. Lever, *Inorganic Electronic Spectroscopy*, 2nd edition, Elsevier Science, Amsterdam, **1984**.
[23] R. Das, K. K. Nanda, K. Venkatsubramanian, P. Paul, K. Nag, *J. Chem. Soc. Dalton Trans.* **1992**, 1253–1257.
[24] D. Dobrzyńska, L. B. Jerzykiewicz, M. Duczmal, A. Wojciechowska, K. Jabłońska, J. Palus, A. Ozarowski, *Inorg. Chem.* **2006**, *45*, 10479–10486.
[25] S. Yamada, *Coord. Chem. Rev.* **1966**, *1*, 415–437.
[26] O. Kahn, *Molecular Magnetism*, VCH-Wiley, Weinheim, **1993**.
[27] V. V. Pavlishchuk, M. Prushan, A. Addison, *Theor. Exp. Chem.* **2005**, *41*, 229–234.
[28] M. J. Prushan, D. M. Tomezsko, S. Lofland, M. Zeller, A. D. Hunter, *Inorg. Chim. Acta* **2007**, *360*, 2245–2254.
[29] E.-G. Jäger, M. Rudolph, *J. Electroanal. Chem.* **1997**, *434*, 1–18.
[30] M. Rudolph, *SpecReg*, Friedrich-Schiller-Universität Jena **2000**.
[31] E.-G. Jäger, K. Schuhmann, H. Görls, *Chem. Ber./Recl.* **1997**, *130*, 1643–1646.
[32] H.-D. Youn, E.-J. Kim, J.-H. Roe, Y. C. Hah, S.-O. Kang, *Biochem. J.* **1996**, *318*, 889–896.
[33] D. P. Barondeau, C. J. Kassmann, C. K. Bruns, J. A. Tainer, E. D. Getzoff, *Biochemistry* **2004**, *43*, 8038–8047.
[34] J. M. McCord, I. Fridovich, *J. Biol. Chem.* **1969**, *244*, 6049–6055.
[35] B. H. J. Blelski, G. G. Shiue, S. Bajuk, *J. Phys. Chem.* **1980**, *84*, 830–833.
[36] Y.-H. Zhou, H. Fu, W.-X. Zhao, W.-L. Chen, C.-Y. Su, H. Sun, L.-N. Ji, Z.-W. Mao, *Inorg. Chem.* **2007**, *46*, 734–739.
[37] S. Nica, M. Rudolph, H. Görls, W. Plass, *Inorg. Chim. Acta* **2007**, *360*, 1743–1752.
[38] *COLLECT*, Data Collection Software, Nonius B. V., Netherlands, **1998**.
[39] *SMART*, Software for the CCD Detektor System, version 5.05: Bruker AXS: Madison, WI, **1998**.
[40] Z. Otwinowski, W. Minor in "Processing of X-ray Diffraction Data Collected in Oscillation Mode", in Methods in Enzymology, Vol. 276, Macromolecular Crystallography, Part A (Eds.: C. W. Carter, R. M. Sweet), Academic Press, San Diego, **1997**, pp. 307–326.
[41] G. M. Sheldrick, SHELXS-97 and SHELXL-97, University of Göttingen, Göttingen (Germany), **1997**.

Received: July 22, 2007
Published online: December 4, 2007

